Reaction Layer Characterization of the Braze Joint of Silicon Nitride to Stainless Steel

R. Xu and J.E. Indacochea

This investigation studies the role of titanium in the development of the reaction layer in braze joining silicon nitride to stainless steel using titanium-active copper-silver filler metals. This reaction layer formed as a result of titanium diffusing to the filler metal/silicon nitride interface and reacting with the silicon nitride to form the intermetallics, titanium nitride (TiN) and titanium silicide (Ti_5Si_3). This reaction layer, as recognized in the literature, allows wetting of the ceramic substrate by the molten filler metal.

The reaction layer thickness increases with temperature and time. Its growth rate obeys the parabolic relationship. Activation energies of 220.1 and 210.9 kJ/mol were calculated for growth of the reaction layer for the two filler metals used. These values are close to the activation energy of nitrogen in TiN (217.6 kJ/mol).

Two filler metals were used in this study, Ticusil (68.8 wt% Ag, 26.7 wt% Cu, 4.5 wt% Ti) and CB4 (70.5 wt% Ag, 26.5 wt% Cu, 3.0 wt% Ti). The joints were processed in vacuum at temperatures of 840 to 900 °C at various times. Bonding strength is affected by reaction layer thickness in the absence of Ti-Cu intermetallics in the filler metal matrix.

Keywords:
braze metal, coefficient of thermal expansion, intermetallics, silicon nitride, reaction layer

1. Introduction

DURING recent years, significant progress has been made in the development of engineering ceramic materials. A new generation of ceramics was developed and is expected to be widely used in structural applications at high temperatures. Silicon nitride (Si_3N_4) is one of the most important materials in this class. A major anticipated application of silicon nitride is in advanced heat engines in which components are expected to operate for long times at elevated temperatures in hostile environments. Silicon nitride has high strength at high temperatures, good thermal stress resistance due to the low coefficient of thermal expansion, and relatively good resistance to oxidation compared to other high-temperature structural materials. This combination of properties can be used to increase operating temperatures. Components currently in use include silicon nitride turbocharger rotors and ceramic caps on push rods.

However, because of its brittle nature, silicon nitride is used together with structural metals, so a strong joint is required. As a consequence, the lack of joining techniques has seriously limited its use. Conventional fusion welding cannot be normally performed to join ceramic to metal due to melting of large regions of the base materials and brittle fracture initiation as a result of the high contraction stresses formed during cooling. In addition, the silicon-based ceramics, such as silicon nitride and silicon carbide, sublimate without melting at normal pressures and therefore should not be subjected to fusion welding. Hence, development of effective techniques for joining ceramic components to metals is a challenging requirement for their successful application in engineering structures (Ref 1-10). An important method of joining ceramics is brazing, which depends on the wetting of liquid braze metals on ceramic surfaces to produce strong bonding. However, it is generally difficult to bond ceramics to metals, because of their primarily ionic or atomic bonds, which exhibit low surface energies, and because conventional braze metals cannot wet the ceramics. Brazing filler metals, which contain an active metal (such as titanium), can dramatically improve wettability by reacting with the ceramic, and recently, Ti-added active filler metals have been widely used in joining ceramics (Ref 11-15). However, wetting and bonding mechanisms become complicated because of the reaction between titanium and ceramics and the formation of a reaction layer (Ref 16). An understanding of those factors responsible for good adhesion between metals and ceramics is of considerable technological importance. Results from thermodynamic and kinetic studies on the formation of the reaction layer were obtained for Cu-Ti filler metals, but details of the growing process of this reaction layer for Ag-Cu-Ti filler metals have not been reported yet (Ref 17-18).

This study focuses on brazing silicon nitride (Si_3N_4) to stainless steel with Ag-Cu-Ti filler metals. In an earlier investigation (Ref 19), results showed that cracks in the Si_3N_4 and reaction layer were related to the brazing processing and microstructure, and that ultimately the strength of Si_3N_4 to stainless steel joints was affected by the cracking behavior, the thickness of the reaction layer, and braze metal morphology. This investigation studies the bonding mechanism, the kinetics of the reaction layer growth at the bonding interface between silicon nitride and Ag-Cu-Ti filler metals, and the mechanical properties of the Si_3N_4 to stainless steel joints.

2. Experimental Procedure

2.1 *Materials and Braze Processing*

Silicon nitride (Si_3N_4), type NCX-34, hot-pressed with Y_2O_3, was sliced in 10 mm × 10 mm × 3 mm pieces and brazed

R. Xu and **J.E. Indacochea,** University of Illinois at Chicago, Civil and Materials Engineering Dept. (m/c 246), Chicago, IL 60680, USA

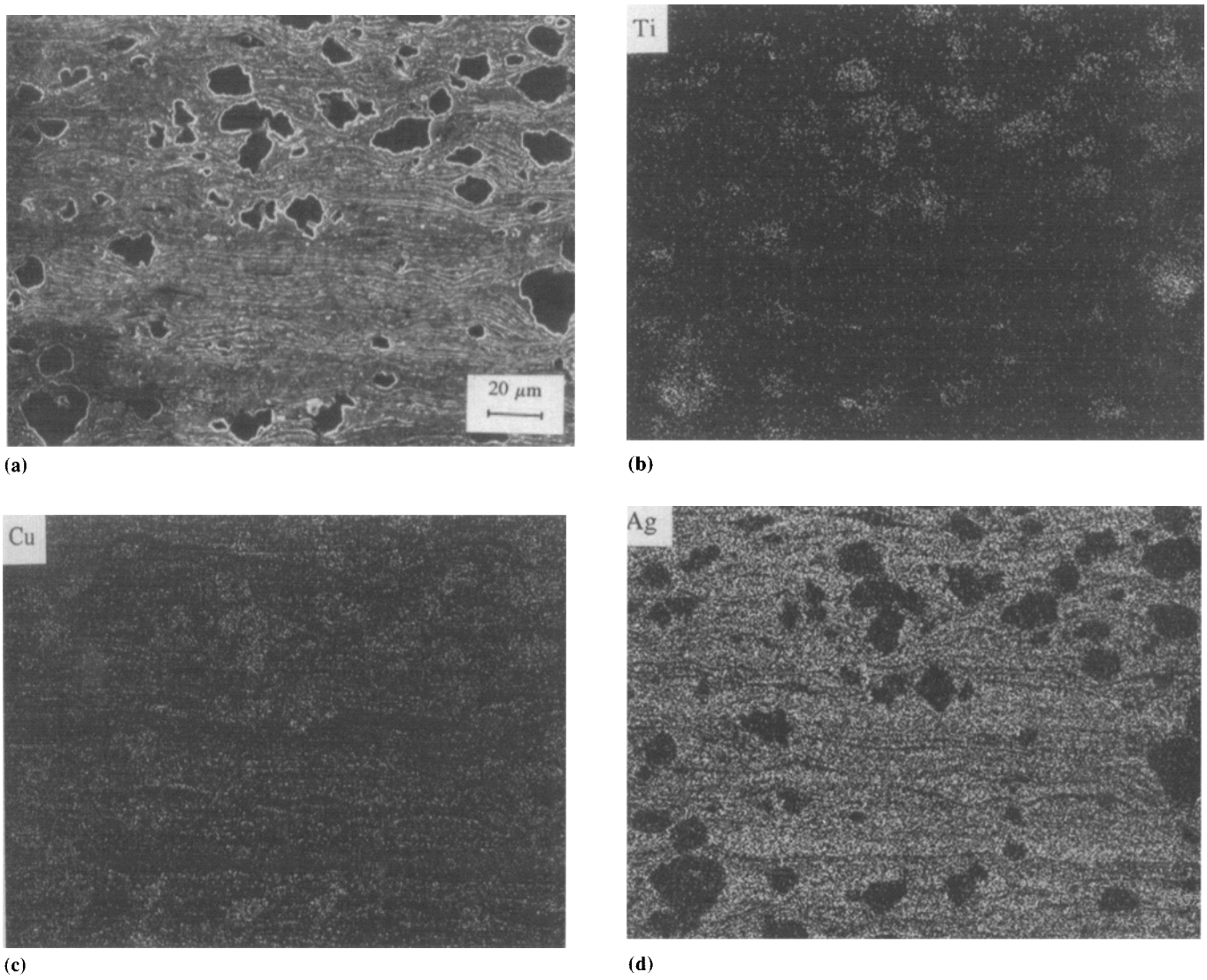

Fig. 1 (a) Scanning electron microscopy micrograph of as-received filler metal, CB4 (70.5Ag-26.5Cu-3.0Ti). (b-d) X-ray elemental maps of as-received filler metal, CB4 (70.5Ag-26.5Cu-3.0Ti)

Table 1 Composition and critical temperatures of the active filler metals

Filler metals	Chemical composition, w%			Liquidus, °C	Solidus, °C
	Ag	Cu	Ti		
Ticusil	68.8	26.7	4.5	850	830
CB4	70.5	26.5	3.0	857	803

to 15 mm diam 410 stainless steel coupons of variable thicknesses. Two kinds of Ag-Cu eutectic filler metals containing Ti, Ticusil, and CB4, were used in the form of foils (1.3 mm thick); their compositions and critical temperatures are listed in Table 1. Furnace brazing was carried out at temperatures of 840 to 900 °C for 6 and 60 min in vacuum. The brazing processing apparatus was composed of a graphite bar resistance furnace, a controller, a vacuum chamber, and a vacuum system, which includes a diffusion pump.

Before brazing, the Si_3N_4 and stainless steel surfaces were manually ground on silicon carbide abrasive papers down to 600 grit and polished on nylon cloths using diamond paste of grades 6 μm and 1 μm with a lubricant. The Si_3N_4, stainless steel, and filler metals were cleaned in acetone using an ultrasonic cleaner and dried thoroughly. The filler metals were cut into 10 mm × 10 mm pieces and placed between the Si_3N_4 and stainless steel substrates. After loading into the furnace, the vacuum chamber was evacuated to less than 5×10^{-5} torr, and the temperature was raised to 780 °C at a heating rate of 10 °C/min and held at this temperature for 12 min. The samples were then heated to the final brazing temperature of 840 to 900 °C at a heating rate of 5 °C/min and held for the required braz-

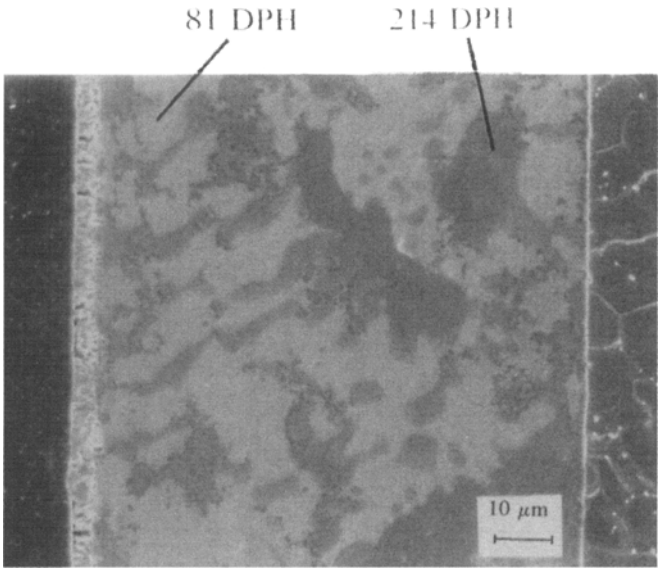

(a)

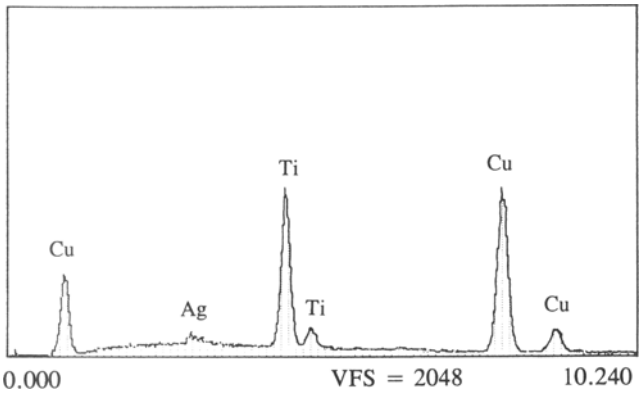

(b)

Fig. 2 (a) Scanning electron microscopy micrograph of Si_3N_4/CB4/stainless steel joints processed at 860 °C for 12 min. (b) Energy dispersive microanalysis on the Ti particles of Si_3N_4/CB4/stainless steel joints processed at 860 °C for 12 min

ing time. After brazing, each test specimen was cooled slowly to room temperature at a rate of 5 °C/min to 500 °C, and then 2 °C/min to room temperature, to reduce the thermal stresses.

2.2 *Microstructure Evaluations*

The brazed specimens were sectioned perpendicular to the Si_3N_4-stainless steel interface and mounted. Samples were prepared using standard metallographic techniques for evaluating the microstructural characterization. Diluted hydrofluoric acid was used to etch the samples.

The microstructure of the joints was determined by optical microscopy and scanning electron microscopy (SEM); the element distribution was resolved by scanning transmission electron microscopy (STEM) with energy dispersive microanalysis (EDX) and x-ray diffractometry (XRD). The thickness of a reaction layer that developed at the filler metal-ceramic substrate

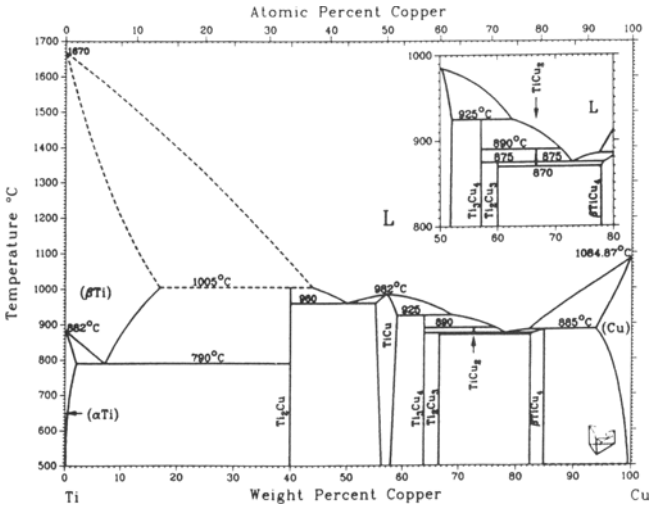

Fig. 3 Ti-Cu binary phase diagram (Ref 20)

interface was measured using optical microscopy and SEM. Because of the unevenness of the reaction layer, an average of five measurements of the thickness was used, and two specimens were measured in each test. SEM and STEM samples were carbon coated for better conductivity.

2.3 *Shear Strength Test*

Mechanical properties of the Si_3N_4 to stainless steel joints were assessed by shear tests. These tests were performed at room temperature at a crosshead speed of 0.5 mm/min using a special mechanical fixture for holding the braze coupons. The shear strength was determined by dividing the fracture load by the cross-section area of the joint.

3. Results and Discussion

3.1 *Microstructure and Elemental Distribution*

The microstructures of the filler metals before brazing were examined to determine if they could affect the processing times and temperatures for producing a sound braze joint. The changes in the braze joint microstructure were monitored metallographically as time and temperature were systematically varied. The initial microstructure of the CB4 filler metal consists of Cu-Ti intermetallic particles homogeneously distributed in a eutectic Ag-Cu matrix (Fig. 1). Semiquantitative EDX spot analysis of the particles shows that these are Ti-rich Ti_2Cu_3 intermetallics; these results were also confirmed by XRD.

During brazing, the Ti_2Cu_3 appears to decompose into a mixture of Ti_3Cu_4 plus liquid richer in Cu. On cooling, the proeutectic Ti_3Cu_4 will remain present and stable at room temperature, while the Cu-rich liquid will undergo a eutectic transformation producing $Ti_2Cu_3 + TiCu_4$. Figure 2(a) shows a light-gray silver-rich matrix with a large, dark-gray second phase and another, much darker, precipitate-like phase. EDX analysis of the large, dark-gray second phase, which included some of the precipitate-like particles, showed an average composition of this region of 8 at.% Cu and 32 at.% Ti. See Fig.

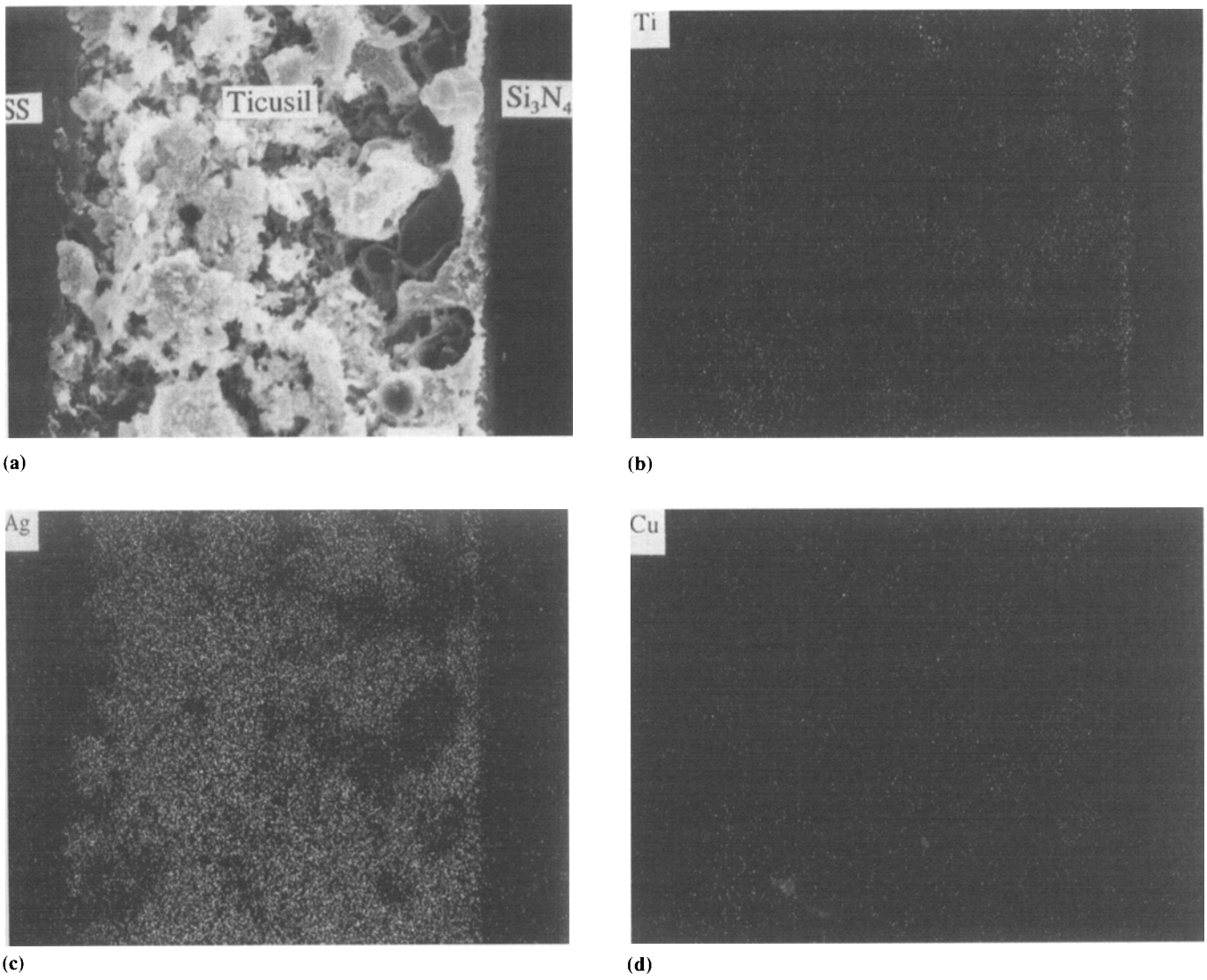

Fig. 4 (a) Scanning electron microscopy micrograph of Si_3N_4/Ticusil/stainless steel joints processed at 860 °C for 12 min. (b-d) X-ray elemental maps of Si_3N_4/Ticusil/stainless steel joints processed at 860 °C for 12 min

2(b). Checking this composition in a partial binary (Ti-Cu) equilibrium phase diagram (Fig. 3) shows that all three phases—Ti_3Cu_4, Ti_2Cu_3, and $TiCu_4$—will almost certainly be present at room temperature. Note that the addition of silver to the filler metal lowers the melting temperature of the alloy. The liquidus temperature is ~850 °C. The joint discussed to explain the morphological and chemical changes was processed at 860 °C for 12 min.

Microstructural evaluation of the CB4 joints brazed at 940 to 860 °C revealed increases of copper-rich Ti-Cu intermetallics in the proeutectic silver phase and in the eutectic Ag-Cu matrix. Some titanium diffused to the Si_3N_4/filler metal interface producing a reaction layer as shown in Fig. 2(a). The joints processed with the CB4 filler metal at 880 to 900 °C show that the titanium-copper particles disappeared, most of the titanium diffused to the Si_3N_4/filler metal interface, and the bulk of the braze layer became a soft Ag-Cu matrix without titanium intermetallic particles.

The microstructure of the as-received Ticusil filler metal consists of a titanium strip-like component sandwiched in between Cu-Ag eutectic matrices, significantly different from the microstructure observed in the CB4 filler metal. EDX analysis reveals the presence of pure Ti in the Ti strip and only Cu and Ag in the eutectic Cu-Ag matrix (Ref 19). The microstructure of the Ticusil joint processed at 840 °C for 30 min showed Cu had diffused into the Ti strip, but this still remained morphologically the same, except that a small amount of Ti had diffused to the Si_3N_4/filler metal interface. The Ti strip broke up as the brazing temperature and time increased; large Ti-rich Ti-Cu particles were observed in the joint processed at 860 °C, as shown in Fig. 4(a). EDX results revealed that the large white matrix was Ag rich and the dark particles were titanium-copper intermetallics, most probably Ti_2Cu_3. See Fig. 4(b-d).

The microstructure found in the joints brazed at higher temperatures (880 to 900 °C) does not contain Ti-Cu particles; it consists of a large reaction layer at the Si_3N_4 interface produced

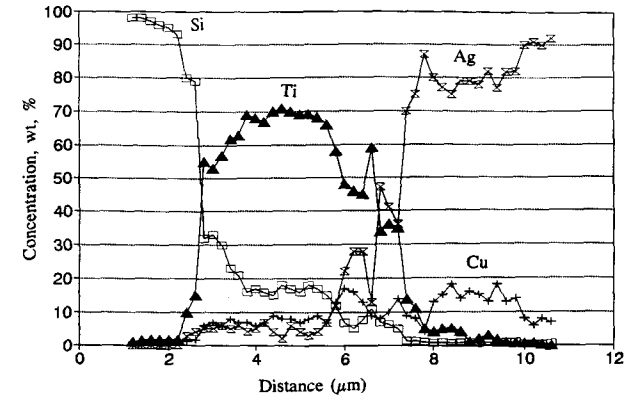

(a)

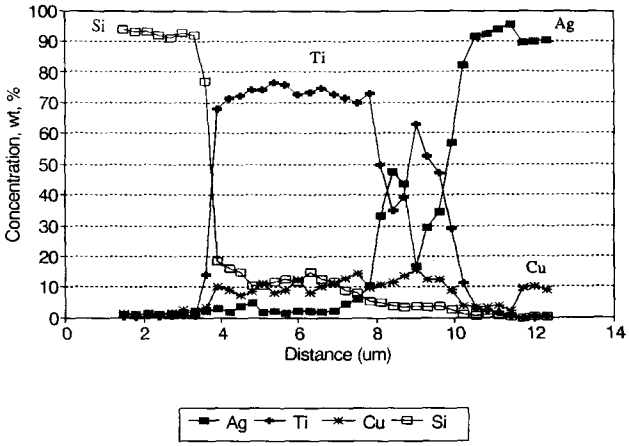

(b)

Fig. 5 (a) Energy dispersive microanalysis composition profiles across the Si_3N_4-Ticusil interface of the Si_3N_4-stainless steel joint with Ticusil. (b) Energy dispersive microanalysis composition profiles across the Si_3N_4-CB4 interface of the Si_3N_4/CB4/stainless steel joint

by a substantial migration of Ti to this location and a Cu-Ag eutectic matrix.

3.2 *Evaluation of the Reaction Layer*

EDX profiles of the reaction layers in the Si_3N_4/Ticusil and Si_3N_4/CB4 interfaces show that the layers are rich in Ti and Si (Fig. 5a and b). STEM (with EDX) analysis indicated that the reaction layers were also rich in N. XRD of the reaction layers confirmed the existence of TiN and Ti_5Si_3, as shown in Fig. 6. Similar reaction products were also found in other studies (Ref 21-25).

The interfacial reaction at the silicon nitride/filler metal interface can be explained by the reduction reaction of the silicon nitride with titanium and the formation of titanium base compounds. According to the Ti-Si-N phase diagram in the temperature range of 700 to 1000 °C (Ref 26), shown in Fig. 7, TiN rather than Si_3N_4 is the stable nitride in contact with pure Ti. Because there are no lines between Si_3N_4 and titanium silicides in the Ti-Si-N phase diagram, titanium silicides are unstable in the presence of Si_3N_4. Titanium is expected to react with Si_3N_4 to form TiN and free Si. This reaction can be represented by:

$$Si_3N_4(s) + 4Ti(l) = 4TiN(s) + 3Si(s)$$
$$\Delta G^0 = -1356 + 0.199T \text{ kJ/mol} \quad \text{(Eq 1)}$$

where T is temperature in Kelvin and ΔG^0 is the standard free energy change of the reaction, which is obtained from thermodynamics data (Ref 27). In the brazing temperature range from 840 to 900 °C, ΔG^0 values are negative, and thermodynamic calculations indicate that <1.0 at.% of Ti in Ag-Cu is enough to form TiN by Eq 1. At a high enough activity of Ti, the product $Ti_5Si_3(s)$ will form according to:

$$5Ti(l) + 3Si(s) = Ti_5Si_3(s)$$
$$\Delta G^0 = -1151.6 - 0.0166T \text{ kJ/mol} \quad \text{(Eq 2)}$$

The line between Ti_5Si_3 and TiN in the Ti-Si-N phase diagram indicates that Ti_5Si_3 is stable in the presence of TiN and Ti, and therefore, this reaction is energetically possible in terms of the standard free energy change in the brazing temperature range selected in this investigation.

Ideally, the activity of titanium should be high to ensure that TiN as well as Ti_5Si_3 is formed for improving wetting and bonding, but titanium concentration should be low enough to inhibit the growth of thick reaction layers. The presence of silver in the alloy increases the Ti activity coefficient in the Ag-Cu-Ti melts significantly. Titanium in the eutectic Ag-Cu melt showed a positive deviation from ideal solution behavior, and its activity coefficient was ~6.5 relative to pure solid Ti (Ref 28).

Figure 8 shows the morphology of the reaction layer at the Si_3N_4/filler metal interface and reveals two layers in the reaction layer. The layer adjacent to the Si_3N_4 (inner) layer, which was very thin (~1 μm thick), was expected to be composed mainly of TiN. The other layer (outside) between the inner layer and filler metal was composed of TiN and Ti_5Si_3. The thickness of this layer was ~5 μm. This result was confirmed by x-ray photoelectron spectroscopy of the Si_3N_4 and Ti-Ag-Cu filler metal interface (Ref 29). After the inner reaction layer has formed at the interface, nitrogen and silicon could diffuse through the reaction layer and react with titanium to form the TiN and Ti_5Si_3 reaction layer.

3.3 *A Wetting Assessment*

The negative Gibbs free energy changes of the chemical reactions described above are expected to contribute to the driving force of wetting. In the absence of any reaction, whether or not the liquid wets the solid is determined by the relative magnitudes of the interfacial energies. The driving force for wetting is given by $\gamma_{sv} - \gamma_{sl}$, shown in Fig. 9, which is represented in the Young-Dupre equation:

$$\gamma_{sv} - \gamma_{sl} = \gamma_{lv} \cos\theta \quad \text{(Eq 3)}$$

where γ_{sv}, γ_{sl}, and γ_{lv} are interfacial energies between the solid-vapor, solid-liquid, and liquid-vapor, and θ is the wetting angle.

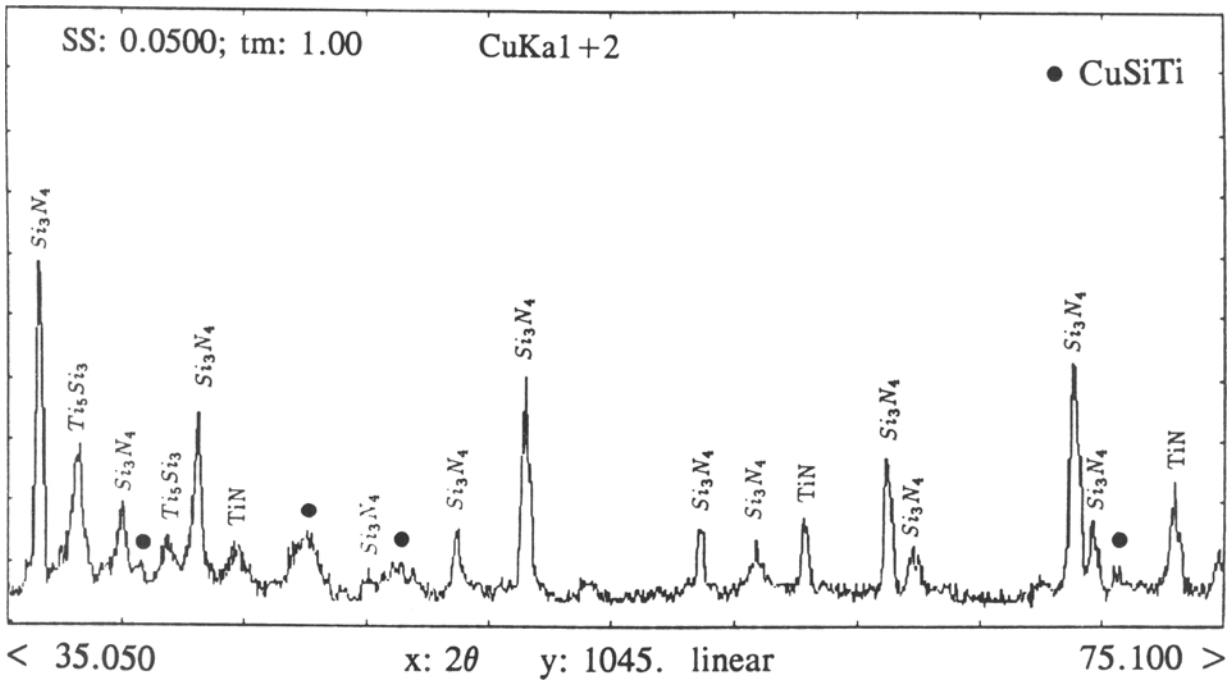

Fig. 6 X-ray diffraction pattern of the reaction layer in the

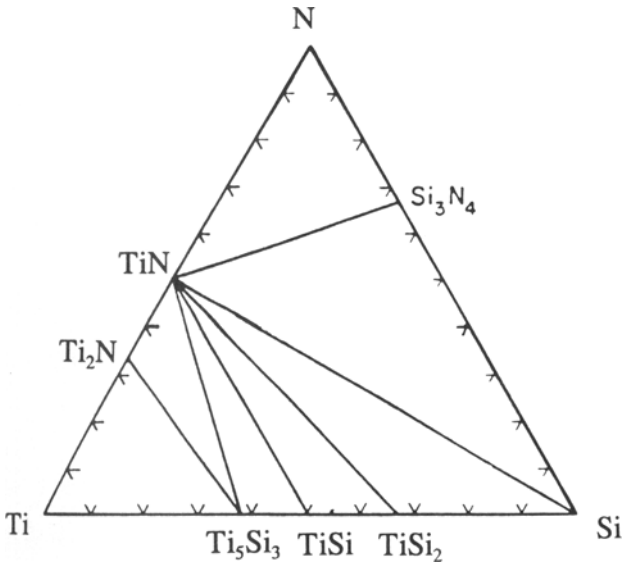

Fig. 7 Ti-Si-N phase diagram in the temperature range 700 to 1000 °C (Ref 26)

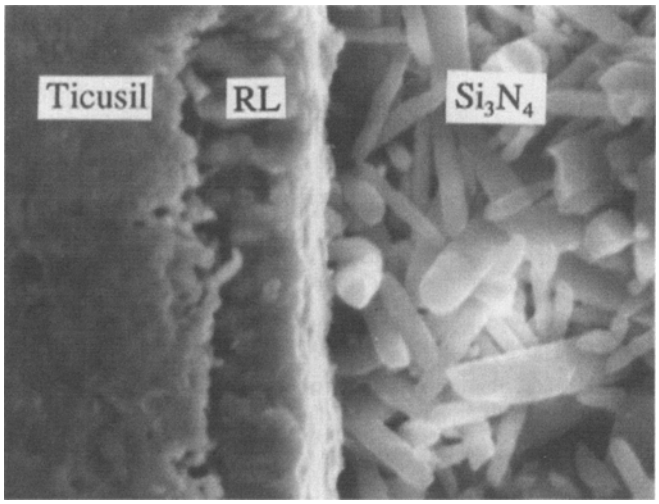

Fig. 8 Scanning electron microscopy micrograph of Si_3N_4/Ticusil/stainless steel joints processed at 860 °C for 30 min and etched in molten NaOH at 350 °C for 8 min

However, if there are reactions between the liquid and the solid, the driving force for wetting is related to the Gibbs energy change of the reaction and the interfacial energy changes (Ref 30):

$$F_{wet} = C\,\Delta G + \gamma(\theta) \qquad \text{(Eq 4)}$$

where F_{wet} is the driving force for wetting, ΔG is the Gibbs energy of the reaction, C is a constant related to the stoichiometry

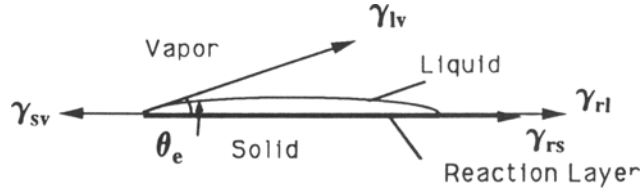

Fig. 9 Schematic of solid wet by liquid of nonreaction and reaction wetting mechanism

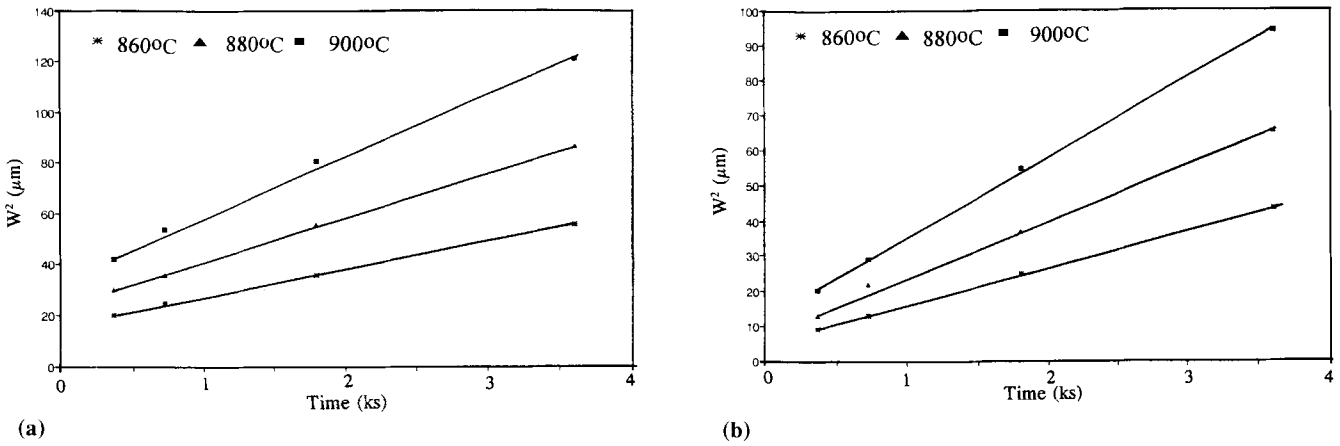

Fig. 10 (a) Relation between the reaction layer thickness and brazing time of parabolic growth rate at the Si_3N_4-Ticusil interface. (b) Relation between the reaction layer thickness and brazing time of parabolic growth rate at the Si_3N_4-CB4 interface

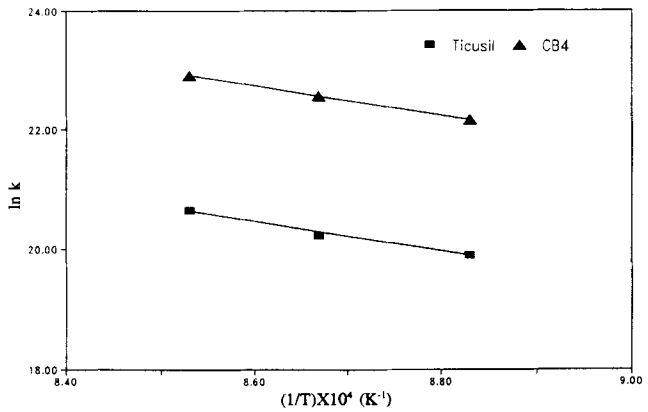

Fig. 11 Relation between the parabolic rate constant and brazing temperatures

of the reaction, and $\gamma(\theta) = \gamma_{rl} + \gamma_{rs} - \gamma_{sv} + \gamma_{lv}\cos\theta$, as shown in the Appendix.

When the reactions reach equilibrium, the driving force for wetting is minimized to zero and the wetting angle is θ_e.

$$\gamma_{sv} - (\gamma_{rl} + \gamma_{rs}) - C\,\Delta G = \gamma_{lv}\cos\theta_e \qquad \text{(Eq 5)}$$

The above equation shows that θ_e will be decreased when the interfacial reaction occurs, resulting in improved wetting.

3.4 *Reaction Layer Kinetics*

After the initial reaction layer is formed at the filler metal/silicon nitride interface, additional silicon and nitrogen, which did not react with titanium at the original interface, could diffuse through the reaction layer to the filler metal and react with titanium to form additional TiN and Ti_5Si_3, resulting in growth of the reaction layer. The growth of the reaction layer was controlled by diffusion of an element or elements in the reaction layer, which can be treated by the reaction diffusion concept. The change in the reaction layer thickness with variation in brazing temperature and time was examined to study the diffusion mechanism. The straight lines in Fig. 10(a) and (b) imply that the growth rate of the reaction layers for both Ticusil and CB4 joints obey the parabolic relationship:

$$X^2 = 2kt \qquad \text{(Eq 6)}$$

where X is the thickness of the reaction layer (μm), t is the brazing time (s), and k is the parabolic rate constant (μm²/s), which is related to temperature, $k = A_o\exp(-Q/RT)$, where Q is activation energy in kJ/mol, T is absolute temperature in K, A_o is a constant, and R is gas constant.

Therefore, the following equation indicates that the activation energy could be calculated from the slope of the straight line in the logarithmic plot of k versus $(1/T)$.

$$\ln k = (-Q/R)(1/T) + \ln(A_o) \qquad \text{(Eq 7)}$$

The straight lines for the Ticusil and CB4 filler metal joints shown in Fig. 11 have nearly the same slopes, and activation energies of 220.1 and 210.9 kJ/mol for Ticusil and CB4 filler metal joints, respectively, were obtained from the figures. These values are very close to the activation energy of the diffusion of nitrogen in TiN (Q = 217.6 kJ/mol) as reported in Ref 31. The growth of the reaction layer for the Ticusil and CB4 joints was apparently controlled by the diffusion of nitrogen through the reaction layer. The joints processed with the CB4 filler metal reached the same reaction layer thickness in a shorter time than those produced with Ticusil filler metal at the same brazing temperature because the solidus temperature of CB4 filler metal is lower than that of Ticusil.

3.5 *Mechanical Evaluation of the Joints*

The joint strength was measured in this study for a fixed ceramic-to-metal thickness ratio of 0.3. Figure 12 shows the shear strengths of the braze joints with Ticusil as a function of processing temperature for three different times. For all the braze joints produced at 840 °C, the joint strength was small (18 to 25 MPa), but the increase of brazing temperature from 840 to 880 °C improved the joint shear strength significantly. The shear

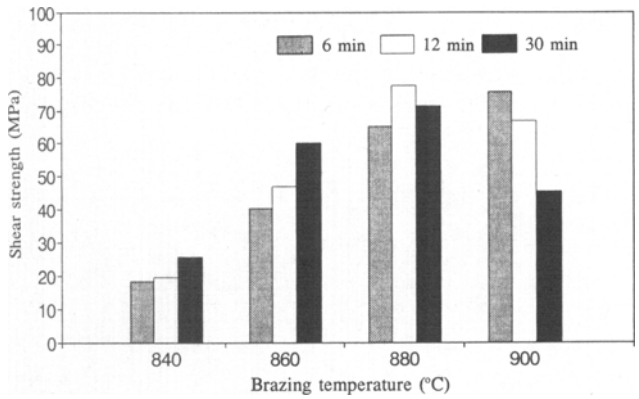

Fig. 12 Shear strength of Si_3N_4/stainless steel joints with Ticusil as a function of processing time and temperature (ratio of Si_3N_4 to stainless steel thickness: 0.3)

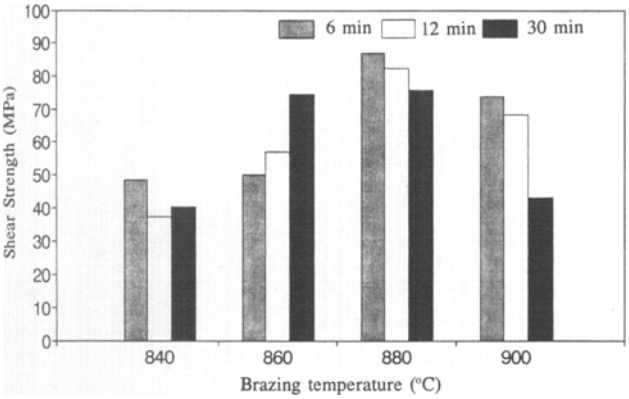

Fig. 13 Shear strength of Si_3N_4/stainless steel joints with CB4 as a function of processing time and temperature (ratio of Si_3N_4 to stainless steel thickness: 0.3)

strength was also affected by brazing time; for example, the increase of brazing time from 6 to 30 min at 860 °C improved the joint shear strength greatly. The Ticusil braze joints produced at 880 °C for 12 min showed the largest shear strength of 78 MPa. The increase in processing time at 880 °C from 12 to 30 min resulted in a slight decrease of strength and a more significant decrease at 900 °C. Such variations in strength can be correlated with changes in the braze metal microstructure and reaction layer thickness. In order to obtain a high joining strength, there should be no brittle phases, such as Ti-Cu, present in the braze metal after brazing. For example, in the joint processed at 840 °C, the Ti strip still remained in the filler metal. However, in the joints with 860 °C processing temperature, the Ti strip did break up, but Ti-Cu particles still were present in the matrix. The microstructure of the joints processed at 880 and 900 °C shows that the Ti strip completely broke up and no Ti-Cu intermetallic particles were found in the filler metal while Ti mostly diffused to the reaction layer. However, the bonding strength was not only affected by the filler metal morphology, but also by the reaction layer thickness. The increase of the reaction layer beyond a certain thickness resulted in the decrease of the bonding strength. Therefore, the decrease in joint strength caused by the increase in processing time at 880 °C from 12 to 30 min and at 900 °C from 6 to 30 min is most probably due to excessive reaction layer thickness.

The CB4 joint strength was carried out to compare the joint strength between the two filler metals investigated in this study. Figure 13 shows the results of the shear strength tests of the CB4 joints as a function of processing temperature for 6, 12, and 30 min. The shear strength of all the CB4 joints processed at 840 °C showed low values (37 to 48 MPa), but higher than the Ticusil braze joints in which the Ti strip existed. The increase of brazing time from 6 to 30 min at 860 °C improved the joint shear strength, but resulted in a slight decrease in strength at 880 °C and more significant decrease at 900 °C. The processing time of 6 min at 880 °C for the CB4 joint appears to be long enough to produce a sound joint (86 MPa) with a braze metal microstructure free of Ti hard particles that could embrittle the braze joint. The braze joints produced at 900 °C had lower shear strengths than those processed at 880 °C. The mechanical behavior of the 900 °C/CB4 braze joints is influenced again by the thickness and possibly the cracking condition of the reaction layer (Ref 19). Higher bonding strength was obtained when the reaction layer was relatively thin.

4. Conclusion

- A reaction layer, which consists of TiN and titanium silicide, developed at the interface between Si_3N_4 and braze metal of the Ticusil or CB4 joints. During brazing, Ti in molten Ticusil or CB4 filler migrated and reacted with Si_3N_4 by: $Si_3N_4(s) + 4Ti(l) = 4TiN(s) + 3Si(s)$, and $5Ti(s) + Si(s) = Ti_5Si_3(s)$. The Gibbs energy changes of the reactions are the driving forces for wetting.
- The growth rate of the reaction layers obeys the parabolic relationship. The activation energies for growth of the reaction layers at the joining interfaces of Ticusil and CB4 joints are 220.1 and 210.9 kJ/mol, respectively, and are close to the activation energy of the diffusion of nitrogen in TiN (217.6 kJ/mol). The growth of the reaction layers was controlled by the diffusion of N in TiN.
- Braze processing with CB4 metal takes less time than with Ticusil metal for the same brazing temperature. Bonding strength was affected by microstructure changes in the filler metal and the reaction layer. Higher bonding strength was obtained when no brittle phases, such as Ti-Cu, were present in the braze metal after brazing and the reaction layer was relatively thin. Optimum brazing parameters were 880 °C/12 min with Ticusil and 880 °C/6 min with CB4.

5. Appendix

Earlier work (Ref 32 and 33) treated the wetting of metal surfaces by molten solder (metal-metal system) where a pure solid metal, A, was assumed wetted by a pure liquid metal, B, resulting in the formation of an intermetallic compound, C, having the stoichiometry A_xB_y. This approach to wetting was applied to three systems, Cu-Sn, Cu-Sb, and Cu-Cd; however, less work was done on ceramic-metal wetting.

In the case of reaction joining systems, where chemical reactions occur at the metal-ceramic interface, the free energy change is associated with both the ΔG_r and the surface energies involved. During the joining of Si_3N_4 with Ag-Cu-Ti filler metals, it is assumed that Ti will dissolve in Ag-Cu liquid and migrate to the Si_3N_4 surface. The initial reaction at the Si_3N_4/filler metal interface is expected to proceed according to Eq 1. The molar relationships can be correlated by:

$$-dn_{Si_3N_4} = -(1/4)dn_{Ti(l)} = (1/4)dn_{TiN} = (1/3)dn_{Si} \quad \text{(Eq 1)}$$

and

$$dn_{Si_3N_4} = (D_{Si_3N_4} / M_{Si_3N_4})dV_{Si_3N_4} \quad \text{(Eq 2)}$$

where dn_{Ti} moles of Ti and $dn_{Si_3N_4}$ moles of Si_3N_4 were transferred into dn_{TiN} moles of TiN and dn_{Si} moles of Si. $D_{Si_3N_4}$, $M_{Si_3N_4}$, and $V_{Si_3N_4}$ are the density, molecular weight, and volume of Si_3N_4, respectively.

When a circular drop spreads an incremental distance (Fig. 8), dr, Gibbs free energy change, dG, at constant temperature and pressure is related to the combination of chemical work and surface work (Ref 34):

$$dG = \Sigma\mu_i dn_i + \Sigma\gamma_i dA \quad \text{(Eq 3)}$$

From Eq 3:

$$\Sigma\mu_i dn_i = [\mu_{Ti}(TiN)dn_{Ti} + \mu_N(TiN)dn_N + \mu_{Si}dn_{Si}] - [\mu_{Ti}(Ti(l))dn_{Ti} + \mu_{Si}(Si_3N_4)dn_{Si} + \mu_N(Si_3N_4)dn_N] \quad \text{(Eq 4)}$$

From Fig. 8:

$$\Sigma\gamma_i dA = (\gamma_{sv} - \gamma_{rl} - \gamma_{rs} - \gamma_{lv}\cos\theta)\, d(\pi r^2) \quad \text{(Eq 5)}$$

where $\mu_N(TiN)$ and $\mu_{Ti}(TiN)$ are the chemical potentials of Ti and N in TiN, $\mu_{Si}(Si_3N_4)$ and $\mu_N(Si_3N_4)$ are the chemical potentials of Si and N in Si_3N_4, and μ_{Si} and $\mu_{Ti}(Ti)$ are the chemical potentials of free Si and Ti in filler metal. γ_{sv} and γ_{lv} are the surface energies of Si_3N_4 (solid) and filler metal (liquid), whereas γ_{rl} and γ_{rs} are the energies of the reaction layer-filler metal and reaction layer-Si_3N_4 interfaces. A and r are the area and the radius of the circular drop, respectively.

Substituting Eq 1, 4, and 5 into 3:

$$dG = [4\mu_{Ti}(TiN) - 4\mu_N(TiN) - 3\mu_{Si}] - [4\mu_{Ti} - 4\mu_N(Si_3N_4) - 3\mu_{Si}(Si_3N_4)]\, dn_{Si_3N_4} + 2\pi r(\gamma_{sv} - \gamma_{rl} - \gamma_{rs} - \gamma_{lv}\cos\theta)dr \quad \text{(Eq 6)}$$

or

$$dG = [2\pi r l_{TiN}(d_{Si_3N_4} / M_{Si_3N_4})dr]\Delta G_r + 2\pi r\gamma(\theta)dr \quad \text{(Eq 7)}$$

where ΔG_r is the Gibbs energy of the reaction, and $\gamma(\theta)$ is surface energy function:

$$\Delta G_r = [4\mu_{Ti}(TiN) + 4\mu_N(TiN) + 3\mu_{Si}] - [4\mu_{Ti} + 4\mu_N(Si_3N_4) + 3\mu_{Si}(Si_3N_4)] \quad \text{(Eq 8)}$$

and

$$\gamma(\theta) = (\gamma_{sv} - \gamma_{rl} - \gamma_{rs} - \gamma_{lv}\cos\theta) = \gamma_{lv}(\cos\theta_e - \cos\theta) \quad \text{(Eq 9)}$$

The equilibrium wetting angle, θ_e, is always less than θ; therefore from Eq 9, $\gamma(\theta)$ must be positive.

$$\cos\theta_e = \frac{\gamma_{rl} + \gamma_{rs} - \gamma_{sv}}{\gamma_{lv}} \quad \text{(Eq 10)}$$

Assume the driving force for wetting, F_{wet} is in accordance with a Gibbs energy change of the system:

$$F_{wet} = \frac{1}{2\pi r}\frac{dG}{dr} \quad \text{(Eq 11)}$$

Hence, substituting Eq 7 into 11:

$$F_{wet} = C\Delta G_r + \gamma(\theta) = \sigma + \gamma(\theta) \quad \text{(Eq 12)}$$

where C is a constant related to the stoichiometry of the reaction.

$$C = \frac{d_{Si_3N_4}}{M_{Si_3N_4}} l_{TiN} \quad \text{(Eq 13)}$$

$$\sigma = C\Delta G_r \quad \text{(Eq 14)}$$

When the interfacial reactions reach equilibrium, the driving force for wetting is minimized to zero, and the wetting angle becomes θ_e; that is:

$$F_{wet} = 0 \quad \text{(Eq 15)}$$

and

$$\theta = \theta_e \quad \text{(Eq 16)}$$

Then Eq 16 becomes:

$$C\Delta G_r + \gamma(\theta_e) = 0 \quad \text{(Eq 17)}$$

But substituting Eq 9 into 17:

$$C\Delta G_r + \gamma_{sv} - \gamma_{rl} - \gamma_{rs} - \gamma_{lv}\cos\theta_e = 0 \quad \text{(Eq 18)}$$

or

$$\gamma_{sv} - \gamma_{rl} - \gamma_{rs} + C\Delta G_r = \gamma_{lv}\cos\theta_e \quad \text{(Eq 19)}$$

Equation 19 indicates that θ_e decreases when the interfacial reaction occurs; wetting is consequently improved.

References

1. A.J. Moorhead, *Weld. J.*, Vol 62 (No. 10), 1984, p 17-22
2. M. Naka, T. Tanaka, I. Okamoto, and Y. Arata, *Trans. JWRI*, Vol 12 (No. 2), 1983, p 177-180
3. M. Naka, K. Sampath, I. Okamoto, and Y. Arata, *Trans. JWRI*, Vol 12 (No. 2), 1983, p 181-183
4. A.J. Moorhead and H. Keting, *Welding J.*, Vol 65 (No. 10), 1980, p 17-31
5. A.J. Moorhead, *Adv. Ceram. Mater.*, Vol 2 (No. 2), 1987, p 159-166
6. H. Mizuhara, E. Huebel, and T. Oyama, *Am. Ceram. Soc. Bull.*, Vol 68 (No. 9), 1989, p 1591-1599
7. X.S. Ning, K. Suganuma, A. Koreeda, and Y. Miyamoto, *J. Mater. Sci.*, Vol 24, 1989, p 2879-2883
8. C.H. Hsueh and A.G. Evans, *J. Am. Ceram. Soc.*, Vol 68 (No. 5), 1985, p 241-248
9. K. Suganuma, T. Okamoto, and M. Koizumi, *Communications of the Am. Ceram. Soc.*, Dec 1984, p c-256 to c-257
10. P.A. Wall and M. Ueki, *J. Am. Ceram. Soc.*, Vol 75 (No. 9), 1992, p 2491-2497
11. A.G. Varias, Z. Suo, and C.F. Shih, *J. Mech. Phys. Solids*, Vol 39 (No. 7), 1991, p 963-986
12. D.H. Kim, S.H. Hwang, and S.S. Chun, *Ceram. Int.*, Vol 16, 1990, p 333-347
13. M.G. Nicholas, D.A. Mortimer, L.M. Jones, and R.M. Crispin, *J. Mater. Sci.*, Vol 25, 1990, p 2679-2689
14. R.R. Kapoor and T.W. Eagar, *J. Am. Ceram. Soc.*, Vol 72 (No. 3), 1989, p 448-454
15. J.H. Selverian and S. Kang, *Weld. J.*, Vol 71 (No. 1), 1992, p 25s-33s
16. R.E. Loehman, A.P. Tomsia, J.A. Pask, and S.M. Johnson, *J. Am. Ceram. Soc.*, Vol 73 (No. 3), 1990, p 552-558
17. M. Naka, I. Okamoto, and Y. Arata, *Mater. Sci. Eng.*, Vol 98, 1988, p 407-410
18. Y. Nakao, K. Nishimoto, and K. Saida, *Trans. Jpn. Weld. Soc.*, Vol 20 (No. 1), 1989, p 66-76
19. R. Xu, J.E. Indacochea, and S. Harren, *Proc. of 3rd Inter. Conf. on Brazing, High Temperature Brazing and Diffusion Welding*, Aachen, Germany, Nov 1992
20. J.L. Murray, Ti-Cu, *Binary Alloy Phase Diagrams*, T.B. Massalski, Ed., American Society for Metals, Metals Park, OH, 1986
21. D.H. Kim, S.H. Hwang, and S.S. Chun, *J. Mater. Sci.*, Vol 26, 1991, p 3223-3234
22. A.P. Xian and Z.Y. Si, *J. Mater. Sci.*, Vol 25, 1990, p 4483-4487
23. K. Suganuma, T. Okamoto, Y. Miyamiti, M. Shimada, and M. Koizumi, *Mater. Sci. Technol.*, Vol 2, 1986, p 1156-1161
24. A.E. Morgan, E.K. Broadbent, and D.K. Sadana, *Appl. Phys. Lett.*, Vol 49 (No. 19), 1986, p 1236-1238
25. J.C. Barbour, A.E.T. Kuiper, M.F.C. Willemsen, and A.H. Reader, *Appl. Phys. Lett.*, Vol 50 (No. 15), 1987, p 953-955
26. R. Beyers and R. Sinclair, *J. Vac. Sci. Technol.*, Vol B2 (No. 4), 1984 Oct-Dec, p 781-784
27. L. Kaufman, Coupled phase diagrams and thermochemical data for transition metal binary systems-III, *Calphad*, Vol 2 (No. 2), 1977, p 117-146
28. J.J. Pak, M.L. Santella, and R.J. Fruehan, *Metall. Trans. B*, Vol 21, 1990, p 349-355
29. Y. Shichi, M. Arita, and M. Matsunaga, Study of Joining Interface Between Si_3N_4 and Ag-Cu-Ti Active Metal, *J. Ceram. Soc. Jpn.*, Vol 96 (No. 9), 1988, p 930-934
30. C.H.P. Lupis, *Chemical Thermodynamics of Materials*, North-Holland, 1983, p 351
31. W.W. Smeltzer and J.G. Desmaison, *Nitrogen Ceramics*, F.L. Riley, Ed., 1977, p 219-235
32. L. Zakraysek, Intermetallic Growth in Tin-Rich Solders, *Weld. J.*, Vol 37(No. 11), 1972, p 536s-541s
33. E.K. Ohriner, Intermetallic Formation in Soldered Copper-Based Alloys at 150 to 250 °C, *Weld. J.*, Vol 66 (No. 7), 1987, p 191s-202s
34. A.W. Adamson, Physical Chemistry of Surfaces, New York, John Wiley & Sons, Inc., Fifth Edition, 1990